Density-functional study of atomic and electronic structures of multivacancies in silicon carbide

Jun-Ichi Iwata,[*] Chikara Shinei,[†] and Atsushi Oshiyama[‡]
Department of Applied Physics, The University of Tokyo, Hongo, Tokyo 113-8656, Japan
(Received 21 September 2015; revised manuscript received 11 February 2016; published 3 March 2016)

We report the density-functional calculations that provide a firm theoretical framework to identify the multivacancies and unravel the underlying physics in the most stable silicon carbide polytype 4H-SiC. The calculations with the generalized gradient approximation (GGA) for the Si and C monovacancy, V_{Si} and V_{C}, have clarified the significantly lower formation energy of the C vacancy accompanied by the efficient pairing relaxation of the surrounding Si dangling bonds. Our GGA calculation also predicts a stable next-neighbor $V_{\mathrm{C}}V_{\mathrm{C}}$ divacancy which is lower in the formation energy than the usual nearest-neighbor divacancy $V_{\mathrm{C}}V_{\mathrm{Si}}$ discussed in the past. We also perform the calculations with the hybrid functional and confirm the stability of the next-neighbor $V_{\mathrm{C}}V_{\mathrm{C}}$ divacancy. Our calculations indeed clarify that it is possible to detect the $V_{\mathrm{C}}V_{\mathrm{C}}$ with its peculiar hyperfine coupling constants by the electron paramagnetic resonance (EPR) measurements. Based on the structural characteristics and the energetics for the monovacancy, we further propose an extended dangling-bond-counting (EDBC) model to choose the energetically favorable topological network of the vacant sites for the multivacancy. The GGA calculations combined with the EDBC model reveal that V_3 and V_6 are energetically favorable. The stable V_3 is a nearest-neighbor complex of V_{C}-V_{Si}-V_{C}, whereas the V_6 is the high-symmetry V_5 (the central V_{Si} surrounded by four V_{C}) plus a symmetry-breaking next-neighbor V_{C}. We perform the GGA calculations for the electronic structure of such V_3 and V_6 and discuss the possibility of detecting these multivacancies. In particular, the EPR-detected ANN1 center is provisionally identified as the doubly positive trivacancy V_{C}-V_{Si}-V_{C}.

DOI: 10.1103/PhysRevB.93.125202

I. INTRODUCTION

Point defects inevitably exist in semiconductors and play important roles both in technology and science [1,2]. Such point defects as lattice vacancies or interstitial atoms generally induce electron states localized around the defects, with their energy levels being in the fundamental energy gap (deep levels). Those deep levels act as carrier traps and usually lead to degradation of semiconductor devices. Hence structural identification of the deep levels is highly demanded from technology viewpoints [3]. Scientifically, the deep localized state brings forth intriguing properties: It enhances electron-lattice interaction and then occasionally constitutes a Anderson negative U system with Jahn-Teller-type local relaxation [4–7]. The localized nature also induces high- and low-spin states [8–10] hidden in corresponding bulk systems, thus being parts of spintronics and quantum information [11–14].

A lot of effort has been given to identify deep levels in semiconductors microscopically, especially in the premier material Si [1–3,15–17]. During heat treatment of materials, point defects diffuse to aggregate, becoming a complex of vacancies and interstitials [1,2]. Energetics, atomic structures, and electronic properties of those complexes have been less pursued, in particular, for semiconductors other than Si. Here we present our total-energy electronic-structure calculations for multivacancies in silicon carbide (SiC), which is regarded as an emerging material for environment-friendly power electronics [18,19].

SiC is a promising material due to its attractive properties such as the high dielectric breakdown voltage and the high melting temperature [18,20,21]. It is a tetrahedrally bonded covalent semiconductor and exists as many polytypes called 2H (wurtzite), 3C (zinc blende), 4H, 6H, and so forth. The most experimentally common polytype is 4H, which is corroborated by our density-functional calculations: The calculated cohesive energy with the generalized gradient approximation (GGA) by Perdew, Burke, and Ernzerhof (PBE) [22] in the density-functional theory (DFT) [23,24] of the 4H polytype is the largest, followed by 6H, 3C, and 2H with the cohesive-energy decrease of 0.1, 1.0, and 8.0 meV per SiC unit, respectively.

Many experimental and theoretical works have been performed for vacancies and interstitials in SiC. Regarding the carbon monovacancy V_{C} and the Si monovacancy V_{Si}, theoretical calculations based on DFT have revealed the roles of Jahn-Teller distortion and spin polarization [25–27]. A general conclusion of the density-functional calculations in the past [28–32] is that the formation energy of V_{C} is smaller than that of V_{Si} by several eV, indicating the relative abundance of V_{C}. Characteristic features of the monovacancies have been corroborated by the many-body perturbation scheme with GW approximation [33,34]. The existence of the monovacancies have been experimentally confirmed by electron paramagnetic resonance (EPR) [35–40] and deep level transient spectroscopy (DLTS) [40–43] measurements, occasionally combined with the calculations of the hyperfine constants. For instance, the $Z_{1/2}$ center observed by DLTS and the EH7 center observed by EPR are now identified as different charge states of V_{C}, which is considered as a negative-U system [40,41].

As for the interstitial defect, several theoretical calculations [29,31,44–46] have been performed to reveal its structural characteristics and energetics. It is generally speculated that

[*]iwata@ap.t.u-tokyo.ac.jp
[†]Present address: Electro-Materials Development Department, Bridgestone Corporation, Yokohama 244-8510, Japan.
[‡]oshiyama@ap.t.u-tokyo.ac.jp

2469-9950/2016/93(12)/125202(12)

©2016 American Physical Society

interstitial carbon atoms gather and form clusters. Their experimental identification has not been done, however.

Thermal treatment inevitably required in device fabrication causes diffusion of point defects and thus point defects are likely to segregate to be of complex forms. Some deep levels are indeed argued to be the divacancy or the trivacancy: The EPR center named P6/P7 is argued to be the divacancy $V_C V_{Si}$ [47], and then a new level emerging after annealing out the P6/P7 is speculated to be originated from a trivacancy [48]. However, detailed investigation of energetics and electron states of such complex defects is lacking. The purpose of the present paper is to clarify the energetics and electron states of the multivacancy in 4H-SiC, the most common polytype, by the first-principles calculations based on DFT.

We first examine characteristic features of the atomic relaxation and formation energies of the monovacancies, V_C and V_{Si}, and of the divacancies. We find that the next-neighbor divacancy $V_C V_C$ is more stable in most cases than the nearest-neighbor divacancy $V_C V_{Si}$ discussed in the past, depending on the Fermi-level position in the energy gap and on the carbon chemical potential. From the characteristic features of the monovacancy, we construct a simple generic model named the extended dangling-bond-counting (EDBC) model, which allows us to systematically evaluate the formation energies of various multivacancies V_n consisting of n_C carbon vacant sites and n_{Si} silicon vacant sites ($n = n_C + n_{Si}$). The EDBC model allows us to screen a huge number of possibilities of the networks of the vacant sites in V_n. The atomic and electronic structures of plausible multivacancies thus obtained have been examined carefully by density-functional calculations. We find that there is a particular size of V_n which is stable against the dissociation to V_{n-1} and V_{n+1}, i.e., the magic number n. The magic number obtained from the EDBC model is further confirmed by the GGA calculations with the PBE functional.

The organization of this paper is the following. In Sec. II, our density-functional calculations based on the real-space scheme are explained. Calculated results for the monovacancies and the divacancies are presented in Secs. III A and III B, respectively. The EDBC model is introduced and stable pairs (n_C,n_{Si}) in V_n are predicted in Sec. III C. Further, in Sec. III C, the density-functional calculations for the multivacancy V_n ($n = 3,4,5,6,$ and 7) are presented, and 3 and 6 are predicted to be the magic numbers. The electronic structures of the stable V_3 and V_6 are presented in Sec. III D. Our findings are summarized in Sec. IV.

II. METHODOLOGY

To efficiently perform accurate density-functional calculations on the current and future computer architectures, we have adopted a real-space (RS) finite-difference scheme [49–55] in the density functional theory (DFT) combined with the first-principles pseudopotential method [56–58]. We use the PBE functional [22] to the exchange-correlation energy in most cases. To examine the validity of GGA, however, we also use the hybrid functional called HSE06 [59,60] for several divacancies. We have developed a highly efficient computation code named RSDFT [61–63]. In the real-space scheme, discrete grid points are introduced in real space, and the Hamiltonian in the Kohn-Sham (KS) equation in the DFT is expressed as a matrix represented at the grid-point space. Differential operators for kinetic energy are replaced by finite-difference operators with sufficiently high orders. The typical order in our calculation is 6 using the values of the Kohn-Sham orbitals at 13 neighboring grid points along one direction. The Hamiltonian matrix therefore becomes sparse and fast-Fourier transformation (FFT) is not required for the Hamiltonian operation. FFT generally causes a heavy communication burden among all the compute nodes in the conventional plane-wave basis-set scheme. Although the real-space scheme is free from the FFT in principle, the current implementation of RSDFT uses FFT for nonlocal exchange operations in hybrid functional calculations. Therefore, to keep the high performance, we perform the calculations with a small number of parallel processes for FFT by using the mixed-parallelization scheme explained below.

Parallelization is performed by dividing the unit cell into several subregions, and each region is allocated on each compute node. We also divide the compute nodes into several small groups and perform band-index parallelization by using these groups. We have performed a benchmark test for a 107 292-atom Si nanowire system with 82 944 nodes of the K computer at the Advanced Institute for Computational Science in Kobe, Japan. We have achieved extremely high performance: 5.48 pFLOPS, corresponding to 51.7% of the peak performance [62,63].

Defects in an otherwise perfect crystal are simulated by a supercell model. A supercell containing 576 lattice sites of 4H-SiC with a defect is arranged periodically. The defect-free supercell is prepared by the full relaxation of the atomic configurations and the volume optimization. Then we introduce defects in the thus obtained supercell and relax atomic configurations until the forces are less than 5×10^{-2} eV/Å. The formation energy defined below converges within 20 meV by this optimization process with the 576-site supercell.

The formation energy $E_f^{(q)}(V_n)$ of the multivacancy V_n consisting of n_{Si} silicon vacant sites and n_C carbon vacant sites with the charge state q is defined as

$$E_f^{(q)}(V_n) = E_D^{(q)} - E_X + \mu_{Si} n_{Si} + \mu_C n_C + q(\varepsilon_v + \varepsilon_F), \quad (1)$$

where $E_D^{(q)}$ and E_X are total energies of the supercells with and without the charged defect, respectively. μ_{Si} and μ_C are chemical potentials of Si and C atoms, respectively, and the electron chemical potential is expressed by the Fermi energy ε_F measured from the valence-band top ε_v. The Si and C chemical potentials satisfy a relation,

$$\mu_{Si} + \mu_C = \mu_{SiC}, \quad (2)$$

where μ_{SiC} is the total energy of 4H-SiC per SiC molecular unit. We define a C-rich (Si-poor) condition in which diamond carbon can precipitate ($\mu_C = \mu_{C\,\mathrm{diamond}}$) and a C-poor (Si-rich) condition in which diamond-structured Si can precipitate ($\mu_{Si} = \mu_{Si\,\mathrm{diamond}}$). We examine the variation of the formation energy as a function of the chemical potential of the atom. Our GGA calculations show that the possible range of the chemical potential $\Delta\mu_C$ is 0.51 eV.

The stable charge state of the defect changes with varying ε_F. The occupancy level $\varepsilon(q_1/q_2)$ is defined as the Fermi-level position in the gap at which the stable charge state changes

between q_1 and q_2 [6,64]. This is obtained as a value of ε_F where $E_f^{(q_1)}(V_n) = E_f^{(q_2)}(V_n)$. The occupancy level $\varepsilon(q_1/q_2)$ is close to the Kohn-Sham (KS) level in the gap for the defect with the corresponding charge in the usual cases.

In order to evaluate the value of the valence-band top ε_v in (1), several schemes have been proposed [65]. Here we adopt a scheme [66] based on Janak's theorem [67] and an ansatz of the linearity of the density-functional total energy as a function of the fractional charge [68–70]. In this scheme, we use the total energies of the charged defect-free supercells. For negatively charged defects, we introduce the conduction-band bottom ε_c instead of ε_v, and thus use the band gap ε_{gap}. (Details are given in the Appendix.) Hence, for the negatively charged defects, we encounter the band-gap problem in the standard approximations in DFT [71]. Hybrid functionals in DFT shows a trend in improving the band-gap problem [72]. We also perform hybrid calculations using the HSE06 functional [60] for the divacancy and confirm essential features obtained by the PBE functional.

In the supercell model for the charged defect, we have to put the homogeneous counter charge to keep the supercell system neutral in order to avoid the divergence of the total energy. Hence we need to make a correction for the total energy due to this artificial background charge [71]. To evaluate the correction for the electrostatic energy, we simply adopt a point and homogeneous charge model [73] and have obtained the correction of $9q^2/(10\epsilon R)$, where ϵ and R are the dielectric constant of SiC ($\epsilon = 9.7$ in this paper) and the dimension of the supercell ($R = 21.0$ bohr in our supercell model), respectively. To search diffusion pathways and corresponding energy barriers, we adopt a constrained minimization technique in which a mutidimensional vector connecting initial and final geometries is introduced and, on each multidimensional plane perpendicular to the vector, the geometry optimization is performed. By this procedure, we reach the saddle-point geometry between the initial and final geometries and obtain the corresponding energy barrier.

Using the obtained KS orbitals of the deep levels, we calculate hyperfine coupling (hf) constants with neighboring nuclei. This requires the amplitude of the target Kohn-Sham orbital at the corresponding nuclear site. We thus adopt the projector augmented wave method [74]. The computations of the hf constants are performed using the Vienna Ab initio Simulation Package (VASP) [75,76].

III. RESULTS AND DISCUSSION

A. Monovacancy

There are two inequivalent lattice sites in 4H-SiC: One is of local cubic symmetry (k site hereafter) and the other is of hexagonal symmetry (h site hereafter). The formation energies of the monovacancy for the k and h sites are close to each other with the variance of 0.12 eV. We have found deep levels mainly characterized as dangling-bond (DB) states of the surrounding atoms. Due to the difference in the electron affinity between C and Si, the position of these dangling-bond states is different, leading to the difference in the occupancy levels between V_{Si} and V_C. All of these features are in agreement with the previous works [26,29–31,34].

TABLE I. Calculated formation energies (in unit of eV) of the neutral multivacancy V_n under the C-poor condition. E_f and E_f^0 are the formation energies obtained by GGA for the relaxed and unrelaxed geometries, respectively. The values E_f^{EDBC} obtained by the extended dangling-bond-counting (EDBC) model are also shown. The superscripts k and h denote the vacant sites of the cubic and hexagonal symmetry. Note that E_f^{EDBC} is independent of the symmetry of the vacant site.

n	Vacancy	E_f^{EDBC}	E_f	E_f^0
1	V_C^k		3.74	4.87
1	V_C^h		3.87	4.91
1	V_{Si}^k		7.64	8.24
1	V_{Si}^h		7.56	8.23
2	$V_C^h V_{Si}^h$	8.81	7.06	7.76
2	$V_C^k V_C^k$	7.60	6.11	7.58
2	$V_C^h V_C^h$		6.46	7.34
2	$V_C^k V_C^h$		6.17	7.55
3	$V_C^k V_{Si}^h V_C^h$	10.02	7.25	8.22
3	$V_C^k V_{Si}^h V_C^k$		7.29	8.38
3	$V_C^h V_{Si}^k V_C^h$		7.39	8.49
4	$V_C^k V_C^k V_C^k V_{Si}^h$	11.23	8.69	10.22
4	$V_C^k V_C^k V_C^h V_{Si}^h$		8.71	10.16
5	$V_C^k V_C^k V_C^k V_C^h V_{Si}^h$	12.44	10.59	12.63
5	$V_C^h V_C^h V_C^h V_C^k V_{Si}^k$		10.62	11.97
6	$V_C^h V_C^h V_C^h V_C^k V_{Si}^k V_C^h$	13.8	11.07	13.63
6	$V_C^k V_C^k V_C^k V_C^h V_{Si}^h V_C^k$		10.96	14.34
6	$V_C^k V_{Si}^h V_C^k V_{Si}^h V_C^k V_{Si}^h$	17.01	14.85	17.74
6	$V_C^h V_{Si}^k V_C^h V_{Si}^k V_C^h V_{Si}^k$		14.56	17.36

There are two important features of the formation energies of the monovacancy. First, the formation energy of V_C is much smaller than that of V_{Si} (see Table I below): The formation energy of the neutral unrelaxed V_C is 4.87 eV (5.38 eV) at the k site and 4.91 eV (5.42 eV) at the h site in the C-poor (C-rich) condition, whereas the corresponding formation energy of V_{Si} is 8.24 eV (7.73eV) at the k site and 8.23 eV (7.73eV) at the h site in the C-poor (C-rich) condition. This means that the formation of the C dangling bond costs a lot compared with the Si dangling bond, which comes from the larger cohesive energy of diamond compared with the diamond-structured Si.

Second, the relaxation of neighboring atoms enhances the imbalance in the formation energy. In V_C, each two of the four Si DBs forms a pair, as shown in Figs. 1(a) and 1(b). As a result, the energy gain upon relaxation in V_C is $1.04 \sim 1.13$ eV depending on the k and h site. On the other hand, in V_{Si}, the neighboring C atoms are unable to form the pairs with the nearby C because of its small covalent radius: The bond length of C in diamond is 1.5 Å, whereas the bond length in SiC is 1.9 Å. The relaxation of the surrounding C atoms in V_{Si} is thus the small breathing relaxation. We have found that they show outward relaxation of 0.2 Å. Instead, V_{Si} with its neutral charge state shows the spin polarization ($S = 1$) due to the exchange interaction of two electrons in the deep level. The energy gain is found to be $0.61 \sim 0.68$ eV depending on the k and h site. These larger pairing and smaller breathing energy gains render the formation energy of V_C to be substantially lower.

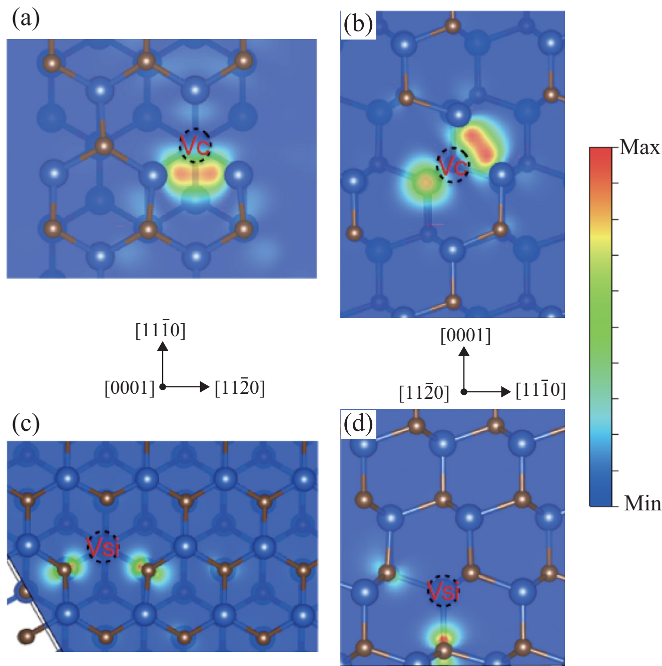

FIG. 1. Geometry optimized structures and the contour plot of the highest occupied Kohn-Sham (KS) orbitals of (a),(b) carbon vacancy V_C and (c),(d) silicon vacancy V_{Si}. Blue (large) and brown (small) spheres depict Si and C atoms, respectively. The KS levels are located in the energy gap and the amplitude squared of the orbitals are represented as contour plots.

This imbalance in the formation energy between V_C and V_{Si} is an important factor to discuss the stability of the multivacancy.

B. Divacancy

Isolated monovacancies tend to aggregate through heat treatment to overcome diffusion barriers. The first product is the divacancy. In SiC, the deep centers, P6/P7, detected by EPR measurements are identified as the neutral divacancy, $V_C V_{Si}$ [47], though it was suggested to be the pair of V_C and the C antisite previously [77].

In this section, we first present the calculated results for the divacancy $V_C V_{Si}$ to examine the validity of the GGA (PBE) functional in comparison with the hybrid (HSE06) functional. We take the axial divacancy in which both C and Si vacancies are located at h sites [78]. Figure 2 shows the calculated formation energies of the axial $V_C V_{Si}$ as a function of the Fermi energy ε_F. We have found that $+1$, neutral, -1 (not shown), and -2 charge states appear depending on the ε_F position. The HSE results agree almost quantitatively with the previous HSE results using a 96-atom super cell [14]. The formation energy obtained by the PBE functional with the experimental band gap (see Appendix) is slightly smaller (0.15–0.22 eV) than that obtained by the HSE06 functional for the charged states. For the neutral state, however, the obtained value with the PBE functional is smaller than that by the HSE06 functional by 0.81 eV. This difference causes the shifts of the occupancy levels by a half eV.

As for the spin states and the atomic relaxations, the PBE and the HSE functionals provide identical results. The Kohn-Sham level structures near the energy gap are schematically

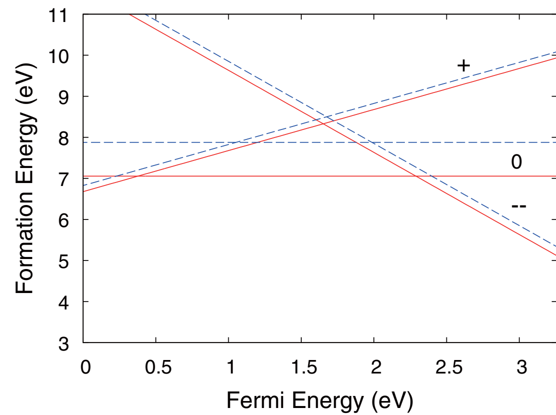

FIG. 2. Formation energy of the neutral (0), positively charged (+), and double negatively charged (−−) axial divacancy $V_C V_{Si}$ as a function of the Fermi energy in the energy gap measured from the valence-band top. The red solid and the blue dashed lines are obtained by the PBE and the HSE06 functionals, respectively. In the PBE calculations, the experimental band gap is used to obtain the formation energy for the negatively charged defect.

shown in Fig. 3(a). The spin states are found to be $S = 1/2, 1$, and 0 for the $+1$, neutral, and -2 states, respectively. For the neutral $V_C V_{Si}$, the characteristic atomic relaxation takes place: The nearest-neighbor three Si atoms and also the nearest-neighbor three C atoms exhibit inward breathing relaxation, forming almost regular Si- and C-atom triangle configurations. The amount of the breathing is quite different for Si and C. The Si-Si and the C-C distances in the triangles are 3.02 Å (2.99 Å) and 3.19 Å (3.17 Å), respectively, in the HSE (PBE) calculations.

From the comparative calculations described above, we conclude that the PBE calculations provide, at least qualitatively, the same results as with the HSE calculations. Hence we present the PBE results hereafter, unless otherwise stated.

We may consider that the formation energy of the vacancy is evaluated by counting the number of the dangling bonds that are generated [dangling-bond-counting (DBC) model] [79], i.e., the formation energy is the energy cost to generate the DBs. In this sense, the nearest-neighbor pair of V_C and V_{Si} seems to be energetically favorable since such pairing minimizes the number of the DBs in V_2: six DBs in the nearest-neighbor pair vs eight DBs in the next-neighbor pair.

This is not necessarily true in SiC, however. As described in Sec. III A, the formation of a C DB costs a lot compared with

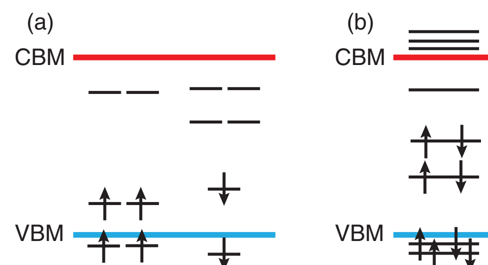

FIG. 3. Schematic illustration of the Kohn-Sham levels near the energy gap for the divacancies. The neutral (a) axial $V_C V_{Si}$ and (b) $V_C V_C$ with the vacancies at the k and h sites.

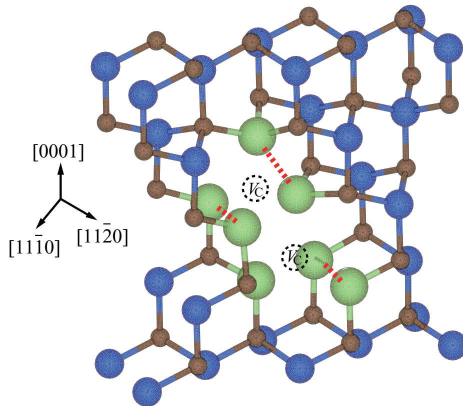

FIG. 4. Geometry optimized structure of the divacancy $V_C V_C$ composed of a next-neighbor pair of two carbon vacancies. Blue (large) and brown (small) spheres depict Si and C atoms, respectively. The nearest-neighbor Si atoms around $V_C V_C$ are marked by Green (large) spheres. The vacant sites are depicted by the dashed circles. The two nearest-neighbor Si atoms connected by the red dashed line form the pairing relaxation.

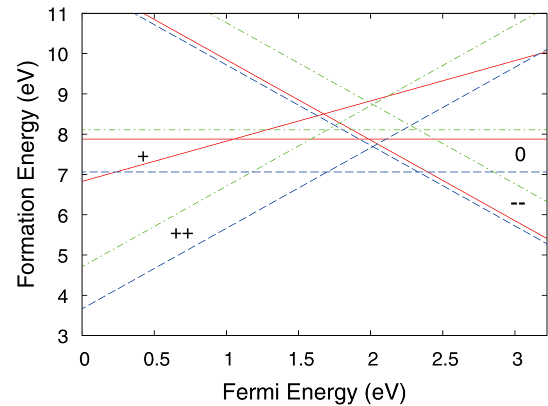

FIG. 6. Formation energies of the axial divacancy $V_C V_{Si}$ (red solid lines) and the next-neighbor divacancy $V_C V_C$ (blue dashed and green dot-dashed lines) calculated with the HSE06 functional. For $V_C V_C$, the two vacant sites are the k and h sites. The formation energies for the neutral (0), positively charged (+), double positively charged (++), and double negatively charged (−−) states are shown. The results under C-poor (blue dashed lines) and C-rich (green dot-dashed lines) conditions are shown.

the cost for Si DBs. It is thus plausible to form two carbon vacancies located at the next-neighbor sites, $V_C V_C$ (Fig. 4). Figure 5 shows the calculated formation energies of $V_C V_C$ as a function of the Fermi energy ε_F. We have found that the divacancy $V_C V_C$ exists as doubly positive, neutral, and negative charge states depending on the ε_F position. The positive charge state is only metastable for any position of ε_F in the energy gap.

To examine the relative stability (i.e., abundance) of the nearest-neighbor divacancy $V_C V_{Si}$ and the next-neighbor divacancy $V_C V_C$, we have performed the HSE calculations. Figure 6 shows the formation energies of the two types of divacancies as a function of the Fermi-level position under both C-poor and C-rich conditions. Under a C-poor condition, we have found that the next-neighbor divacancy $V_C V_C$ is energetically favorable compared with the $V_C V_{Si}$ for any position of the ε_F in the gap. The occupancy level $\varepsilon(++/0)$ is located at the midgap, whereas $\varepsilon\,(0/-)$ appears at $\varepsilon_C - 0.89$ eV. Even under the C-rich condition, $V_C V_C$ is more stable than $V_C V_{Si}$ when ε_F is located in the lower half of the energy gap. Doubly positive charged $V_C V_C$ exists as the most stable divacancy for $\varepsilon_F \leqslant \varepsilon_v + 1.59$ eV. This unusual stability of the next-neighbor divacancy originates from the large difference in the formation energy between the Si and C vacancies.

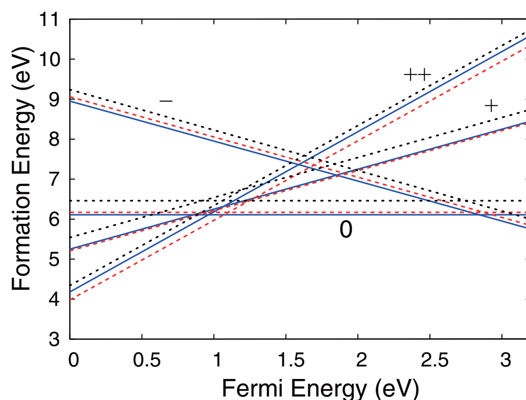

FIG. 5. Formation energy of the neutral (0), positively charged (+), double positively charged (++), and negatively charged (−) divacancy $V_C V_C$ under C-poor condition as a function of the Fermi energy in the energy gap measured from the valence-band top. The blue solid, red dashed, and black dotted lines represent the formation energies of $V_C V_C$ located at one cubic- and one hexagonal-symmetry sites, two cubic-symmetry sites, and two hexagonal-symmetry sites, respectively. The results are obtained by the PBE functional.

In the $V_C V_{Si}$ divacancy, there are two almost degenerate deep levels in the energy gap (Fig. 3). In the neutral $V_C V_{Si}$, the lower degenerate level originating mainly from carbon DBs is doubly occupied and become a spin-triplet state, as is already shown in Ref. [14]. The $V_C V_C$ divacancy shows a different feature. As shown in Fig. 4, six of the seven nearest-neighbor Si atoms form three rebonds by pairing-type relaxation. The relaxation energy is more than 1 eV (Table I). As a result of the relaxation, the eight DBs are mixed and become two resonant levels in the valence band, three resonant levels in the conduction band, and three levels in the gap (Fig. 3). Then, in the neutral state, the lower two deep levels are occupied with four electrons, thus becoming a spin-singlet state. The positively charged and negatively charged states are therefore active in EPR measurement.

The +1 and −1 charged $V_C V_C$ divacancies exist as either the stable state or the metastable state (Figs. 5 and 6). Then EPR measurements with or without photoexcitation can generally measure this divacancy. We have indeed found several occupancy levels in the energy gap. Calculated spin densities for positively and negatively charged $V_C V_C$ are shown in Fig. 7. The deep (Kohn-Sham) level corresponding to the spin density is different between the positively and negatively charged states. This manifests itself in Fig. 7. This difference in the spin density should be measured by the EPR experiment. Table II shows calculated hyperfine coupling constants for $(V_C V_C)^{+1}$ and $(V_C V_C)^{-1}$, which are qualitatively different from each other. Experimental confirmation is awaited.

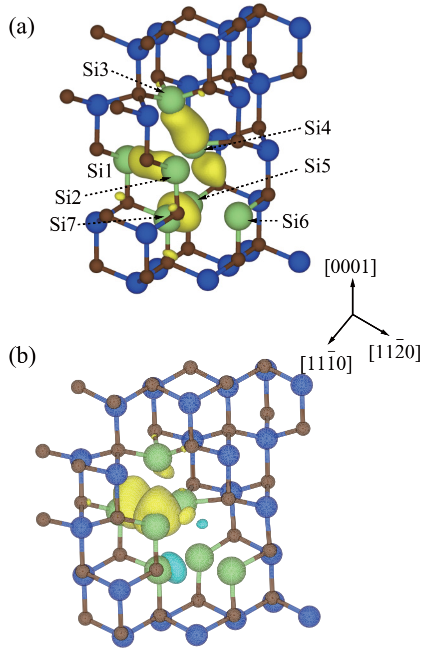

FIG. 7. Calculated spin densities $[n_\uparrow(\boldsymbol{r}) - n_\downarrow(\boldsymbol{r})]$ of the divacancy $V_C^k V_C^h$ for (a) positively and (b) negatively charged states. The superscript here denotes the symmetry (k: cubic; h: hexagonal) of each vacant site. The positive (yellow) and the negative (blue) isovalue surface at 20% of the maximum value is shown. The color code depicting each atom is the same as in Fig. 4. Labels Si1-Si7 denote Si atoms which have dangling bonds before relaxation. The hyperfine constant at each Si site is shown in Table II.

C. Magic number of the multivacancy

Various heat treatments of semiconductors generally produce multivacancies V_n $(n = n_C + n_{Si})$ larger than V_2. The multivacancy with a particular number n has its own nanoscale shape essentially determined by the bond network peculiar to tetrahedrally bonded semiconductors. In Si, e.g., V_n in which compact internal vacant space is formed is predicted to be relatively low formation energy (magic number n): The DBC model predicts that the hexavacancy V_6 and decavacancy V_{10} show lower formation energies [79], and these magic numbers have been confirmed by the density-functional calculations [80] and also by other atomistic calculations [81–83]. In addition to 6 and 10, a systematic tight-binding calculation [84] predicts larger magic numbers such as $n = 14,17,22,26,35$.

In the DBC model, the formation energy E_F of the multivacancy which generates n_{DB} dangling bonds is given as $E_f = n_{DB}E_{DB}$, where E_{DB} is the energy cost to form a DB. In an elemental tetrahedrally bonded material such as Si, E_{DB} is approximately regarded as a half of the cohesive energy per atom.

In SiC, this DBC model needs to be modified since the energy cost to form a Si DB, E_{DB}^{Si}, is much smaller than that to form a C DB, E_{DB}^{C}, as is clarified by the GGA calculations for the monovacancy in Sec. III A. In addition, the GGA calculations have clarified that the relaxation of the nearest-neighbor Si and C atoms is qualitatively different: The nearest-neighbor two Si atoms around the vacancy which are located as the second neighbors to each other form a rebond through the pairing relaxation, gaining the energy of Δ_p; the nearest-neighbor C atom, on the other hand, is unable to form a rebond due to small atomic radius and exhibits outward breathing-type relaxation occasionally accompanied by the spin polarization, gaining the energy of Δ_b. When we consider a particular V_n in SiC, the numbers of dangling bonds of C and Si, n_{DB}^{C} and n_{DB}^{Si}, and the number of the Si pairs, n_p^{Si}, are uniquely determined from the network topology. Hence the formation energy of such multivacancy is evaluated as

$$E_f^{EDBC} = n_{DB}^{Si}E_{DB}^{Si} + n_{DB}^{C}E_{DB}^{C} - n_p^{Si}\Delta_p - n_{DB}^{C}\Delta_b, \quad (3)$$

in our extended dangling-bond-counting (EDBC) model. From our GGA calculations for the monovacancy, the values in the EDBC model are given as $E_{DB}^{Si} = 1.21$ eV, $E_{DB}^{C} = 2.06$ eV, $\Delta_p = 0.26$ eV, and $\Delta_b = 0.16$ eV.

Applying this EDBC model to the divacancy, the formation energy of $V_C V_C$ is lower than that of $V_{Si}V_C$ by 1.2 eV (Table I). This formation-energy difference agrees satisfactorily with our GGA result. Here we emphasize that E_f^{EDBC} is evaluated by using solely the calculated GGA values for the monovacancy.

In the multivacancy V_n, there are various possibilities of n_{Si} and n_C which satisfy $n = n_{Si} + n_C$. We use our EDBC model to search the pair (n_{Si}, n_C) and the topology of the vacant sites, which give the lowest formation energy of V_n. Table I shows E_f^{EDBC} for the thus obtained most stable V_n. We have then performed GGA calculations for these V_n. The atomic relaxation is fully taken into account in the GGA calculations. The GGA values E_f of the formation energies are also shown in Table I. We have found that the EDBC model qualitatively predicts the variation of the formation energy of the multivacancy. The only exception is the hexavacancy in which the formation energy by the GGA calculation is substantially lower than the EDBC model predicts. This is due to the substantial relaxation of the surrounding atoms, which is not described in terms of the pairing or breathing peculiar to the monovacancy (see Sec. III D).

TABLE II. Calculated hyperfine constant (in unit of MHz) at each Si site (depicted in Fig. 7) of $V_C^k V_C^h$ for positively (+1) and negatively (−1) charged states.

Defect	Atom	[11$\bar{2}$0]	[11$\bar{1}$0]	[0001]
(+) $V_C^k V_C^h$	Si1	−84.3	−81.4	−116.8
$S = 1/2$	Si2	−76.2	−73.4	−105.7
	Si3	8.09	7.27	9.1
	Si4	−455.0	−450.3	−507.6
	Si5	−40.0	−39.0	−59.6
	Si6	−40.1	−39.2	−59.9
	Si7	−77.6	−76.2	−88.1
(−) $V_C^k V_C^h$	Si1	−219.5	−216.4	−299.6
$S = 1/2$	Si2	−218.5	−215.6	−298.3
	Si3	3.67	3.51	5.48
	Si4	−52.3	−48.2	−71.4
	Si5	3.66	3.09	6.70
	Si6	3.87	3.32	6.95
	Si7	60.0	56.3	73.9

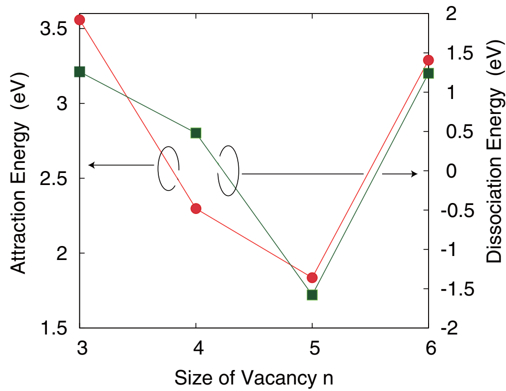

FIG. 8. Dissociation energy ζ (squares) and the attraction energy η (circles) of the multivacancy V_n obtained from GGA calculations. Right and left axes represent ζ and η, respectively.

To discuss the abundance of the multivacancy, the dissociation energy ζ_n defined below is a measure:

$$\zeta_n = E_f(V_{n+1}) + E_f(V_{n-1}) - 2E_f(V_n). \quad (4)$$

This dissociation energy is the energy gain via the reaction from V_{n-1} plus V_{n+1} to $2V_n$, an index showing relative abundance of V_n. In Fig. 8, we show the dissociation energy of V_n obtained by our GGA calculations. Another measure is the attraction energy defined by

$$\eta_n = E_f(V_{n-1}) + E_f(V_1) - E_f(V_n). \quad (5)$$

This is the energy gain via the reaction from V_{n-1} plus V_1 to V_n. The attraction energy η_n of the multivacancy V_n from our GGA calculations is also shown in Fig. 8.

From the dissociation and attraction energies obtained by our GGA calculations, the trivacancy V_3 and the hexavacancy V_6 which have larger ζ and η are considered to be relatively abundant. The magic numbers are 3 and 6 in our GGA calculations. The EDBC model also predicts that the hexavacancy is abundant. However, the trivacancy has smaller dissociation energy in the EDBC model (Fig. 9). This is due to the large relaxation energy in $V_C V_{Si} V_C$, which is properly described by GGA but not by the EDBC model (Table I).

For larger multivacancies, we have calculated the dissociation energies of V_n using the EDBC model, and found that

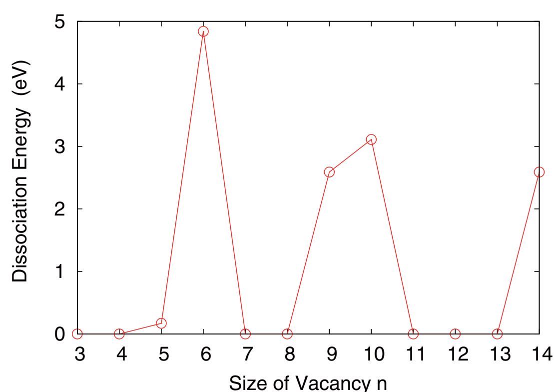

FIG. 9. Dissociation energy ζ of the multivacancy V_n obtained from EDBC calculations.

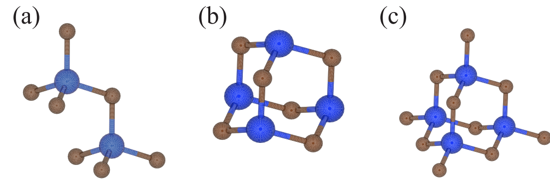

FIG. 10. Geometry of the *vacant* sites in large multivacancy V_n: (a) $n = 9$, (b) $n = 10$, and (c) $n = 14$. The large (blue) and small (brown) spheres depict the *vacant* sites of Si and C, respectively.

$n = 9$, $n = 10$, and $n = 14$ are the magic numbers (Fig. 9). The geometry of V_9, V_{10}, and V_{14} from the EDBC model is shown in Fig. 10. The calculated dissociation energies are 2.59, 3.11, and 2.59 eV, respectively. However, further efforts to determine the relaxed structures are necessary to determine the magic numbers for larger V_n.

D. Tri- and hexavacancies

The dissociation energies presented in the previous section show that the trivacancy V_3 and the hexavacancy V_6 are the relatively abundant multivacancies. In this section, we present atomic and electronic structures of V_3 and V_6 in more detail. The most stable trivacancy consists of two C vacancies and a single Si vacancy located at the sites nearest to each other. The most stable hexavacancy consists of the high-symmetry pentavacancy (the central Si vacancy surrounded by the four nearest C vacancies) and the second-neighbor C vacancy.

Figure 11(a) shows the total-energy minimized structure of the trivacancy V_3 ($V_C^k V_{Si}^h V_C^h$). V_3 is surrounded by undercoordinated 6 Si and 2 C atoms. The 6 Si atoms are grouped in two groups consisting of 3 Si atoms each. The two 3 Si atoms form a rebonded pair, thereby gaining the relaxation energy of about 1 eV (Table I). An EPR center labeled as ANN1 which emerges upon annealing of the divacancy $V_C V_{Si}$ has been provisionally assigned to the trivacancy $V_C V_{Si} V_C$ [48]. This may be in accord with our GGA calculations that show V_3 is energetically favorable.

Figure 12 shows the formation energy of the trivacancy as a function of the Fermi-level position in the gap. We have found occupancy levels $\varepsilon(++/+)$, $\varepsilon(+/0)$, and $\varepsilon(0/-)$ at about 0.4, 0.7, and 2.7 eV, respectively, above the valence-band top. The lower occupancy level corresponds to the KS level with the character of carbon DBs, whereas the upper occupancy level corresponds to the KS level with Si DB character. There are three configurations for $V_3 = V_C V_{Si} V_C$ since there are two inequivalent lattice sites, i.e., h (hexagonal) and k (cubic). For all three configurations, our GGA calculations show that the ground states for doubly positive, positive, neutral, and negative V_3 have the electron spin of $S = 1$, $S = 1/2$, $S = 0$, and $S = 1/2$, respectively. Hence the +2, +1, and −1 charge states are EPR active. Table III shows calculated hyperfine constants for the doubly positive $V_C^k V_C^h V_{Si}^h$. The ANN1 center is not observed in the dark, but emerges under the illumination as a paramagnetic center with $S = 1$. Hence a possibility is that it is a photoexcited +2 state of the trivacancy. Yet further experimental and theoretical efforts are required for the identification of ANN1.

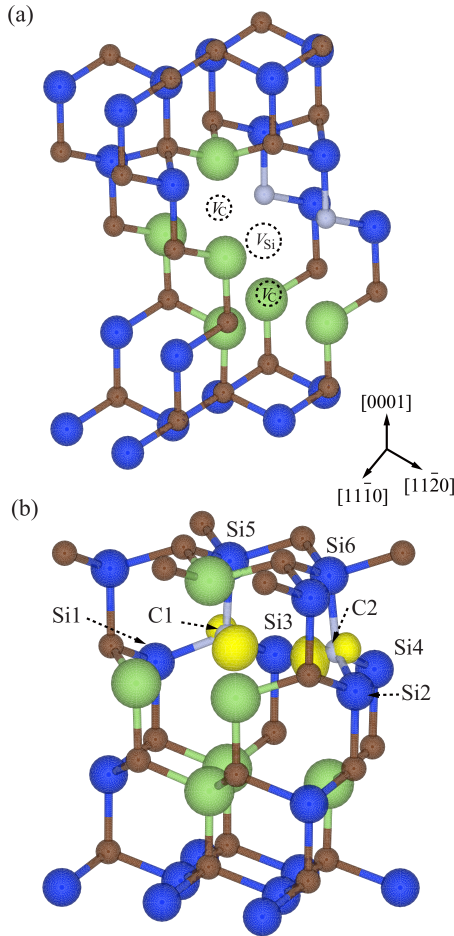

FIG. 11. (a) Geometry optimized trivacancy $V_C^k V_{Si}^h V_C^h$ and (b) its spin density for the positively charged state. The large (green and blue) spheres and the small (brown and light blue) spheres depict Si and C atoms, respectively. The green and light blue atoms are the nearest-neighbor undercoordinated atoms. The dashed circles in (a) depict the vacant sites. The spin density in (b) represented as yellow clouds is an isovalue surface at the 20% of the maximum value. Si1–Si6 and C1–C2 are the labels of the nearest-neighbor atoms for which the hyperfine constants are calculated (Table III).

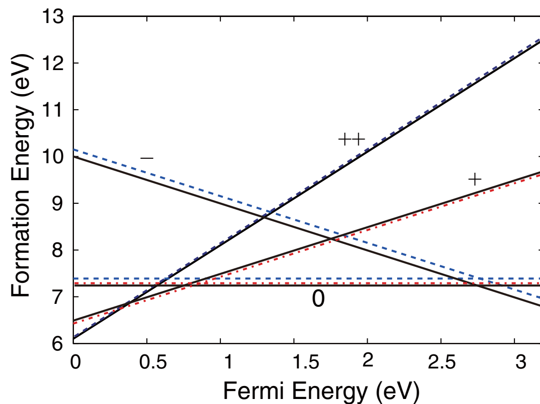

FIG. 12. Formation energies of the trivacancy $V_C V_{Si} V_C$ with several charge states as a function of the Fermi-level position in the gap for the carbon-poor condition. The solid (black), dash-dotted (red), and dashed (blue) lines denote the formation energies of $V_C^k V_{Si}^h V_C^h$, $V_C^k V_{Si}^h V_C^k$, and $V_C^h V_{Si}^k V_C^h$, respectively.

TABLE III. Calculated hyperfine constant (in unit of MHz) of $V_C^k V_C^h V_{Si}^h$ for the doubly positive ++ charge state. The atomic sites from C1 to Si6 are shown in Fig. 11(b).

Defect	Atom	[11$\bar{2}$0]	[11$\bar{1}$0]	[0001]
(++) $V_C^k V_C^h V_{Si}^h$	C1	48.9	49.6	138.3
$S = 1$	C2	49.0	48.6	138.4
	Si1	10.8	9.72	9.1
	Si2	−455.0	−450.3	−507.6
	Si3	−40.0	−39.0	−59.6
	Si4	−40.1	−39.2	−59.9
	Si5	−77.6	−76.2	−88.1
	Si6	−77.6	−76.2	−88.1

The hexavacancy V_6 is also predicted to be relatively stable from our GGA calculations. The most stable form of V_6 is composed of the central Si vacancy surrounded by four C vacancies and the next-neighbor C vacancy, labeled as $V_C^k V_{Si}^k V_C^h V_C^h V_C^h V_C^h$. In the unrelaxed geometry, there are 16 undercoordinated Si atoms around this V_6. We have performed geometry optimization in our GGA calculations The obtained structure is shown in Fig. 13. The DBs in the unrelaxed geometry are totally reorganized. In addition to the pairing-type rebonds, there are resonant-type bonds [17] in which three undercoordinated Si atoms participate. This reconstruction of the DBs produces a large energy gain of 2.6 ∼ 3.4 eV (Table I).

Figure 14 shows the formation energy of the hexavacancy as a function of the Fermi-level position in the gap. We have found that five different charge states are possible: V_6^{++}, V_6^{+}, V_6^{0}, V_6^{-}, and V_6^{--}, among which V_6^{+} and V_6^{-} are metastable. We have found the occupancy levels $\varepsilon(++/0)$ at 1.44 eV above the valence-band top and $\varepsilon(0/--)$ at about 2.76 eV above the valence-band top. The occupancy level $\varepsilon(++/+)$ is almost degenerate with $\varepsilon(++/0)$, whereas the levels $\varepsilon(0/-)$ and $\varepsilon(-/--)$ are almost degenerate with $\varepsilon(0/--)$. We have also examined the interplay between the atomic relaxation and the spin polarization. Our GGA calculations have clarified that the spin of the ground state is $S = 0$ for doubly negative, neutral, and doubly positive charge states,

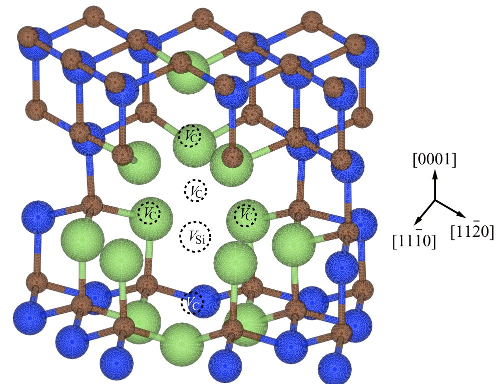

FIG. 13. Geometry optimized hexavacancy $V_C^k V_{Si}^k V_C^h V_C^h V_C^h V_C^h$. The large spheres (blue and green) and small spheres (brown) depict Si and C atoms, respectively. The dashed spheres depict the vacant sites. The green spheres are the nearest-neighbor undercoordinated Si atoms.

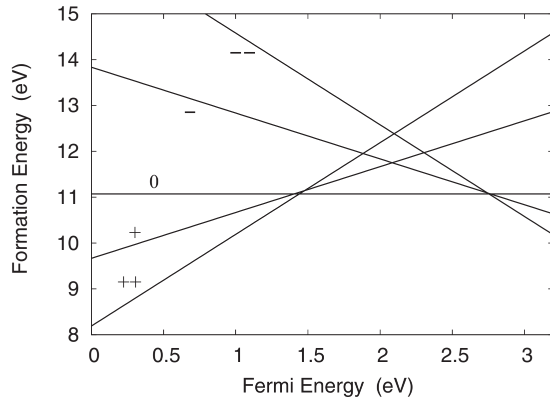

FIG. 14. Formation energies of the hexavacancies V_6 shown in Fig. 13(a) for doubly positive (++), positive (+), neutral (0), negative (−), and doubly negative (−−) charge states as a function of the Fermi-level position measured from the valence-band top in the carbon-poor condition.

whereas it is $S = 1/2$ for the negative and positive charge states.

There are two KS levels which are almost degenerate in the lower half of the energy gap. These two levels accommodate two and four electrons for doubly positive and neutral charge states, respectively. The other two KS levels which are again almost degenerate are located at about 0.6 eV above the aforementioned KS levels. These two levels are occupied by two electrons in the doubly negative charge state.

We have also found that the high-spin state ($S = 1$) emerges as a metastable state for the doubly positive and doubly negative charge states. The energy differences from the ground states are 0.31 and 0.57 eV for V_6^{--} and V_6^{++}, respectively. In Fig. 15, we show the spin densities of these metastable charge states. For a doubly positive charge state, the spin density has amplitude around three Si atoms, each of which has two dangling bonds [Figs. 15(a) and 15(c)]. For a doubly negative charge state, the spin density has amplitude around another three Si atoms, and in this case each Si atom has a single dangling bond [Figs. 15(b) and 15(d)]. This difference in the spin density corresponds to the difference in the KS orbitals mentioned above. The highest occupied KS orbitals for a doubly positive charge state are composed mainly of six DB orbitals of the three Si atoms, and the larger orbital degrees of freedom contribute to lower the orbital energy, compared with another set of almost degenerate KS orbitals related to the doubly negative charge state.

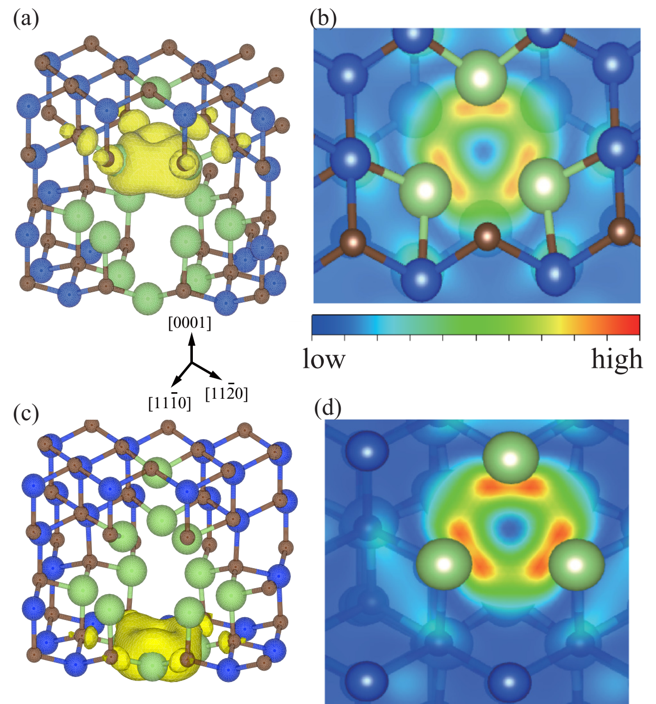

FIG. 15. Spin densities for the (a),(b) doubly positive and (c),(d) doubly negative charge states of the hexavacancy $V_C^k V_{Si}^k V_C^h V_C^h V_C^h V_C^h$. In (a) and (c), the isosurfaces at the value of 20% of the maximum value are shown, and (b) and (d) are the contour plots. The large (blue and green) spheres and the small (brown) spheres depict Si and C atoms, respectively. The green spheres depict the undercoordinated Si atoms.

IV. SUMMARY

We have presented our density-functional calculations that clarify the atomic structures, the energetics, and the electron states of the multivacancy V_n consisting of n_{Si} silicon vacant sites and n_C carbon vacant sites ($n = n_{Si} + n_C$) in the most stable silicon carbide polytype 4H-SiC. The calculations with the generalized gradient approximation (GGA) for the monovacancy, V_{Si} and V_C, have clarified the significantly lower formation energy of the C vacancy accompanied by the efficient pairing relaxation of the surrounding Si dangling bonds. Based on these structural characteristics and the energetics for the monovacancy, we have proposed an extended dangling-bond-counting (EDBC) model to discuss the stability of the multivacancy. The EDBC model predicts a stable next-neighbor $V_C V_C$ divacancy which is lower in the formation energy than the usual nearest-neighbor divacancy $V_C V_{Si}$ discussed in the past. Our GGA calculations have indeed clarified that the $V_C V_C$ is more stable than the $V_C V_{Si}$ under the C-poor condition. Even under the C-rich condition, the next-neighbor divacancy $V_C V_C$ is more stable than the nearest-neighbor $V_C V_{Si}$ when the Fermi level is located in the lower half of the energy gap. The stability of $V_C V_C$ is confirmed by the more sophisticated hybrid-functional calculations. The next-neighbor divacancy can be detected with its peculiar hyperfine coupling constants by the electron paramagnetic resonance (EPR) measurements.

The EDBC model has also been applied to larger multivacancy and has revealed the energetically favorable pair (n_{Si}, n_C) and the topological network for the multivacancy V_n. As a result, V_n with $n = 6,9,10,14$ has been shown to have relatively lower formation energies: the magic numbers of the stable multivacancy. We have also performed GGA calculations for the multivacancy V_n and clarified that V_3 and V_6 are energetically favorable. The stable V_3 is a nearest-neighbor complex of V_C-V_{Si}-V_C, whereas the V_6 is the high symmetry V_5 (the central V_{Si} surrounded by 4 V_C) plus symmetry-breaking next-neighbor V_C. The reason why the EDBC model fails to predict the stability of V_3 is the peculiar relaxation pattern and its large energy gain in V_3 that is properly

taken into account by the GGA calculations but not in the EDBC model.

We have performed the GGA calculations for the electronic structure of the thus obtained stable V_3 and V_6 and discussed the possibility of detecting these multivacancies. We have clarified the existence of various charge states for V_3 and V_6, for which high-spin and low-spin states are possible, depending on the charge states. In particular, the EPR-detected ANN1 center has been provisionally identified as the doubly positive trivacancy V_C-V_{Si}-V_C. The present calculations provide a firm theoretical framework to identify the multivacancies generated by heat treatments of SiC and discuss their physical properties.

ACKNOWLEDGMENTS

This work was supported by the Grants-in-Aid for scientific research under Contract No. 22104005 and also by the "Computational Materials Science Initiative," both conducted by Ministry of Education, Culture, Sports, Science and Technology, Japan. Computations were performed mainly at the Supercomputer Center at the Institute for Solid State Physics, The University of Tokyo, the Research Center for Computational Science, National Institutes of Natural Sciences, and the Center for Computational Science, University of Tsukuba.

APPENDIX

Janak's theorem [67] leads to

$$E(N-1) - E(N) = -\int_0^1 df\ \varepsilon_N(N-1+f), \tag{A1}$$

where $E(N)$ is the total-energy and $\varepsilon_M(N)$ is the Mth Kohn-Sham level of the N-electron system. When we know the "exact" exchange-correlation functional E_{xc}, the total energy should be linear as a function of the fractional occupation number f since such fictitious system should be regarded as a mixed state of N and $N-1$ electron systems. Then, (A1) becomes

$$E(N-1) - E(N) = -\varepsilon_N(N-\delta) = -\varepsilon_N(N-1+\delta), \tag{A2}$$

with δ being an infinitesimal small number. Since the same argument holds for the system with different electron numbers, we have a set of equations such as

$$\begin{aligned} E(N+1) - E(N+2) &= -\varepsilon_{N+2}(N+2-\delta) \\ &= -\varepsilon_{N+2}(N+1+\delta), \end{aligned} \tag{A3}$$

$$E(N) - E(N+1) = -\varepsilon_{N+1}(N+1-\delta) = -\varepsilon_{N+1}(N+\delta), \tag{A4}$$

$$E(N-1) - E(N) = -\varepsilon_N(N-\delta) = -\varepsilon_N(N-1+\delta), \tag{A5}$$

$$\begin{aligned} E(N-2) - E(N-1) &= -\varepsilon_{N-1}(N-1-\delta) \\ &= -\varepsilon_{N-1}(N-2+\delta). \end{aligned} \tag{A6}$$

Note that the current approximations for E_{xc} do not warrant the linearity of the total energy [85].

The formation energy of the multivacancy V_n with the charge state q (electron deficit corresponds to positive q) in SiC is defined in the supercell model as in (1). Then, for a certain V_n,

$$E_f^{(q)}(V_n) - E_f^{(0)}(V_n) = E_D^{(q)} - E_D^{(0)} + q(\varepsilon_v + \varepsilon_F). \tag{A7}$$

Since it is difficult to evaluate the total-energy difference between different charge states in the supercell model, we rewrite the above expression of the formation energy using Eqs. (A3)–(A6).

Suppose a semiconductor contains N electrons in a supercell. Then, from (A5), the valence-band top is

$$\varepsilon_v = \varepsilon_N(N-\delta) = E_X(N) - E_X(N-1), \tag{A8}$$

where $E_X(N)$ is the total energy of the defect-free supercell with N electrons. We also regard the second ionization energy as actually the same as the first ionization energy in condensed matter. Then,

$$\varepsilon_v = \varepsilon_{N-1}(N-1-\delta) = E_X(N-1) - E_X(N-2). \tag{A9}$$

Using (A8) and (A9), we obtain

$$\begin{aligned} &E_f^{(1)}(V_n) - E_f^{(0)}(V_n) \\ &\quad = \left[E_D^{(1)} E_X(N-1)\right] - \left[E_D^{(0)} - E_X(N)\right] + \varepsilon_F, \\ &E_f^{(2)}(V_n) - E_f^{(0)}(V_n) \\ &\quad = \left[E_D^{(2)} - E_X(N-2)\right] - \left[E_D^{(0)} - E_X(N)\right] + 2\varepsilon_F. \end{aligned}$$

More generally, for positive q, we obtain

$$\begin{aligned} E_f^{(q)}(V_n) - E_f^{(0)}(V_n) &= \left[E_D^{(q)} - E_X(N-q)\right] \\ &\quad - \left[E_D^{(0)} - E_X(N)\right] + q\varepsilon_F. \end{aligned} \tag{A10}$$

Here we consider that the ionization energy for the qth electron is equal to ε_v.

For negative q, we use similar treatments as follows. From (A3) and (A4), we obtain

$$\begin{aligned} E_X(N+1) - E_X(N) &= \varepsilon_{N+1}(N+\delta), \\ E_X(N+2) - E_X(N+1) &= \varepsilon_{N+2}(N+1+\delta). \end{aligned}$$

The right-hand sides of the above equations are regarded as the conduction-band bottom ε_c. Then,

$$\begin{aligned} &E_f^{(-1)}(V_n) - E_f^{(0)}(V_n) \\ &\quad = \left[E_D^{(-1)} - E_X(N+1)\right] - \left[E_D^{(0)} - E_X(N)\right] \\ &\qquad - \varepsilon_F + \varepsilon_c - \varepsilon_v \\ &\quad = \left[E_D^{(-1)} - E_X(N+1)\right] - \left[E_D^{(0)} - E_X(N)\right] \\ &\qquad - \varepsilon_F + \varepsilon_{gap}. \end{aligned}$$

Here we introduce the energy gap as

$$\varepsilon_{gap} \equiv \varepsilon_c - \varepsilon_v. \tag{A11}$$

Similarly,

$$\begin{aligned} &E_f^{(-2)}(V_n) - E_f^{(0)}(V_n) \\ &\quad = \left[E_D^{(-2)} - E_X(N+2)\right] - \left[E_D^{(0)} - E_X(N)\right] \\ &\qquad - 2\varepsilon_F + 2\varepsilon_{gap}. \end{aligned}$$

More generally, for negative q, we obtain

$$E_{\mathrm{f}}^{(q)}(V_n) - E_{\mathrm{f}}^{(0)}(V_n) = \left[E_{\mathrm{D}}^{(q)} - E_{\mathrm{X}}(N+q)\right] - \left[E_{\mathrm{D}}^{(0)} - E_{\mathrm{X}}(N)\right] + q\varepsilon_{\mathrm{F}} + q\varepsilon_{\mathrm{gap}}. \tag{A12}$$

We use Eqs. (A10) and (A12) to calculate the formation energy of the defect as a function of the Fermi level in the gap. For the energy gap $\varepsilon_{\mathrm{gap}}$, we use either the theoretical value obtained in the HSE functional or the experimental value in the GGA calculations.

[1] G. D. Watkins, in *Lattice Defects in Semiconductors*, edited by F. A. Huntley (IOP, London, 1975), p. 1.
[2] G. D. Watkins, in *Deep Centers in Semiconductors*, edited by S. T. Pantelides (Gordon and Breach, New York, 1986), p. 147.
[3] For a review, see *Defects in Microelectronic Materials and Devices*, edited by D. M. Fleetwood, S. T. Pantelides, and R. D. Schrimpf (CRC, Boca Raton, FL, 2009).
[4] P. W. Anderson, Phys. Rev. Lett. **34**, 953 (1975).
[5] G. A. Baraff, E. O. Kane, and M. Schlüter, Phys. Rev. Lett. **43**, 956 (1979).
[6] G. A. Baraff, E. O. Kane, and M. Schlüter, Phys. Rev. B **21**, 5662 (1980).
[7] G. D. Watkins and J. R. Troxell, Phys. Rev. Lett. **44**, 593 (1980).
[8] T. Akiyama and A. Oshiyama, J. Phys. Soc. Jpn. **70**, 1627 (2001).
[9] K. Uchida and A. Oshiyama, J. Phys. Soc. Jpn. **79**, 093711 (2010)
[10] Y. Gohda and A. Oshiyama, Phys. Rev. B **78**, 161201(R) (2008).
[11] F. Jelezko, T. Gaebel, I. Popa, A. Gruber, and J. Wrachtrup, Phys. Rev. Lett. **92**, 076401 (2004).
[12] W. F. Koehl, B. B. Buckley, F. J. Heremans, G. Calusine, and D. D. Awschalom, Nature (London) **479**, 84 (2011).
[13] A. L. Falk, B. B. Buckley, G. Calusine, W. F. Koehl, V. V. Dobrovitski, A. Politi, C. A. Zorman, P. X.-L. Feng, and D. D. Awschalom, Nat. Commun. **4**, 1819 (2013).
[14] L. Gordon, A. Janotti, and C. G. Van de Walle, Phys. Rev. B **92**, 045208 (2015).
[15] P. M. Fahey, P. B. Griffin, and J. D. Plummer, Rev. Mod. Phys. **61**, 289 (1989).
[16] O. Sugino and A. Oshiyama, Phys. Rev. Lett. **68**, 1858 (1992).
[17] M. Saito and A. Oshiyama, Phys. Rev. Lett. **73**, 866 (1994).
[18] *Silicon Carbide*, edited by P. Friedrichs, T. Kimoto, L. Ley, and G. Pensl (Wiley-VCH, Weinheim, 2010), Vols. 1 and 2.
[19] J. Rabkowski, D. Peftitsis, and H.-P. Nee, IEEE Indust. Electron. Mag. **6**, 17 (2012).
[20] H. Matsunami, and T. Kimoto, Mater. Sci. Eng. R **20**, 125 (1997).
[21] T. Kimoto and J. A. Cooper, *Fundamentals of Silicon Carbide Technology: Growth, Characterization, Devices and Applications* (Wiley-IEEE, New York, 2014).
[22] J. P. Perdew, K. Burke, and M. Ernzerhof, Phys. Rev. Lett. **77**, 3865 (1996).
[23] P. Hohenberg and W. Kohn, Phys. Rev. **136**, B864 (1964).
[24] W. Kohn and L. J. Sham, Phys. Rev. **140**, A1133 (1965).
[25] P. Deák, J. Miró, A. Gali, L. Udvardi, and H. Overhof, Appl. Phys. Lett. **75**, 2103 (1999).
[26] A. Zywietz, J. Furthmüller, and F. Bechstedt, Phys. Rev. B **59**, 15166 (1999).
[27] A. Zywietz, J. Furthmüller, and F. Bechstedt, Phys. Rev. B **62**, 6854 (2000).
[28] A. Gali, B. Aradi, P. Deák, W. J. Choyke, and N. T. Son, Phys. Rev. Lett. **84**, 4926 (2000).
[29] M. Bockstedte, A. Mattausch, and O. Pankratov, Phys. Rev. B **68**, 205201 (2003).
[30] T. Hornos, A. Gali, and B. G. Svensson, Mater. Sci. Forum **679-680**, 261 (2011).
[31] T. Oda, Y. Zhang, and W. J. Weber, J. Chem. Phys. **139**, 124707 (2013).
[32] X. T. Trinh, K. Szász, T. Hornos, K. Kawahara, J. Suda, T. Kimoto, A. Gali, E. Janzén, and N. T. Son, Phys. Rev. B **88**, 235209 (2013).
[33] M. Bockstedte, A. Marini, O. Pankratov, and A. Rubio, Phys. Rev. Lett. **105**, 026401 (2010).
[34] F. Bruneval and G. Roma, Phys. Rev. B **83**, 144116 (2011).
[35] T. Wimbauer, B. K. Meyer, A. Hofstaetter, A. Scharmann, and H. Overhof, Phys Rev. B **56**, 7384 (1997).
[36] N. Mizuochi, S. Yamasaki, H. Takizawa, N. Morishita, T. Ohshima, H. Itoh, and J. Isoya, Phys. Rev. B **66**, 235202 (2002).
[37] N. Mizuochi, S. Yamasaki, H. Takizawa, N. Morishita, T. Ohshima, H. Itoh, and J. Isoya, Phys. Rev. B **68**, 165206 (2003).
[38] N. Mizuochi, S. Yamasaki, H. Takizawa, N. Morishita, T. Ohshima, H. Itoh, T. Umeda, and J. Isoya, Phys. Rev. B **72**, 235208 (2005).
[39] P. Carlsson, N. T. Son, A. Gali, J. Isoya, N. Morishita, T. Ohshima, B. Magnusson, and E. Janzén, Phys. Rev. B **82**, 235203 (2010)
[40] N. T. Son, X. T. Trinh, L. S. Løvlie, B. G. Svensson, K. Kawahara, J. Suda, T. Kimoto, T. Umeda, J. Isoya, T. Makino, T. Ohshima, and E. Janzén, Phys. Rev. Lett. **109**, 187603 (2012).
[41] K. Kawahara, X. T. Trinh, N. T. Son, E. Janzén, J. Suda, and T. Kimoto, Appl. Phys. Lett. **102**, 112106 (2013).
[42] K. Danno and T. Kimoto, J. Appl. Phys. **100**, 113728 (2006).
[43] Knaeko and Kimoto, Appl. Phys. Lett. **98**, 262106 (2011).
[44] A. Gali, P. Deák, P. Ordejón, N. T. Son, E. Janzén, and W. J. Choyke, Phys. Rev. B **68**, 125201 (2003).
[45] A. Gali, N. T. Son, and E. Janzén, Phys. Rev. B **73**, 033204 (2006).
[46] T. Hornos, N. T. Son, E. Janzén, and A. Gali, Phys. Rev. B **76**, 165209 (2007).
[47] N. T. Son, P. Carlsson, J. ul Hassan, E. Janzén, T. Umeda, J. Isoya, A. Gali, M. Bockstedte, N. Morishita, T. Ohshima, and H. Itoh, Phys. Rev. Lett. **96**, 055501 (2006).
[48] W. E. Carlos, N. Y. Garces, E. R. Glaser, and M. A. Fanton, Phys. Rev. B **74**, 235201 (2006).
[49] J. R. Chelikowsky, N. Troullier, and Y. Saad, Phys. Rev. Lett. **72**, 1240 (1994); J. R. Chelikowsky, N. Troullier, K. Wu, and Y. Saad, Phys. Rev. B **50**, 11355 (1994).
[50] A. P. Seitsonen, M. J. Puska, and R. M. Nieminen, Phys. Rev. B **51**, 14057 (1995).
[51] E. L. Briggs, D. J. Sullivan, and J. Bernholc, Phys. Rev. B **52**, R5471 (1995).

[52] T. Hoshi, M. Arai, and T. Fujiwara, Phys. Rev. B **52**, R5459 (1995).
[53] F. Gygi and G. Galli, Phys. Rev. B **52**, R2229 (1995).
[54] T. Ono and K. Hirose, Phys. Rev. Lett. **82**, 5016 (1999).
[55] J.-I. Iwata, K. Shiraishi, and A. Oshiyama, Phys. Rev. B **77**, 115208 (2008).
[56] G. B. Bachelet, D. R. Hamann, and M. Schlüter, Phys. Rev. B **26**, 4199 (1982).
[57] N. Troullier and J. R. Martins, Phys. Rev. B **43**, 1993 (1991).
[58] D. Vanderbilt, Phys. Rev. B **41**, 7892(R) (1990).
[59] J. Heyd, G. E. Scuseria, and M. Ernzerhof, J. Chem. Phys. **118**, 8207 (2003); J. Heyd and G. E. Scuseria, *ibid.* **120**, 7274 (2004).
[60] A. V. Krukau, O. A. Vydrov, A. F. Izmaylov, and G. E. Scuseria, J. Chem. Phys. **125**, 224106 (2006).
[61] J.-I. Iwata, D. Takahashi, A. Oshiyama, B. Boku, K. Shiraishi, S. Okada, and K. Yabana, J. Comput. Phys. **229**, 2339 (2010). The RSDFT code is available at https://github.com/j-iwata/RSDFT
[62] Y. Hasegawa, J.-I. Iwata, M. Tsuji, D. Takahashi, A. Oshiyama, K. Minami, T. Boku, H. Inoue, Y. Kitazawa, I. Miyoshi, and M. Yokokawa, Intl. J. High Perform. Comput. Appl. **28**, 335 (2014).
[63] Y. Hasegawa, J.-I. Iwata, M. Tsuji, D. Takahashi, A. Oshiyama, K. Minami, T. Boku, F. Shoji, A. Uno, M. Kurokawa, H. Inoue, I. Miyoshi, and M. Yokokawa, *Proceedings of 2011 International Conference for High Performance Computing, Networking, Storage and Analysis* (IEEE SC11, Seattle, WA, 2011) (ACM, New York, NY), Article No. 1.
[64] R. Car, P. J. Kelly, A. Oshiyama, and S. T. Pantelides, Phys. Rev. Lett. **52**, 1814 (1984).
[65] For a review of DFT calculations for defects, see C. G. Van de Walle and J. Neugebauer, J. Appl. Phys. **95**, 3851 (2004).
[66] J.-W. Jeong and A. Oshiyama, Phys. Rev. B **64**, 235204 (2001).
[67] J. F. Janak, Phys. Rev. B **18**, 7165 (1978).
[68] J. P. Perdew, R. G. Parr, M. Levy, and J. L. Balduz Jr., Phys. Rev. Lett. **49**, 1691 (1982).
[69] J. P. Perdew and M. Levy, Phys. Rev. Lett. **51**, 1884 (1983).
[70] L. J. Sham and M. Schlüter, Phys. Rev. Lett. **51**, 1888 (1983).
[71] C. W. M. Castleton, A. Höglund, and S. Mirbt, Phys. Rev. B **73**, 035215 (2006), and references therein.
[72] Y. I. Matsushita, K. Nakamura, and A. Oshiyama, Phys. Rev. B **84**, 075205 (2011), and references therein.
[73] P. E. Blöchl, Phys. Rev. B **62**, 6158 (2000).
[74] P. E. Blöchl, Phys. Rev. B **50**, 17953 (1994).
[75] G. Kresse and J. Hafner, Phys. Rev. B **49**, 14251 (1994).
[76] G. Kresse and J. Furthmuller, Phys. Rev. B **54**, 11169 (1996).
[77] T. Lingner, S. Greulich-Weber, J.-M. Spaeth, U. Gerstmann, E. Rauls, Z. Hajnal, Th. Frauenheim, and H. Overhof, Phys. Rev. B **64**, 245212 (2001).
[78] There are four combinations of vacant sites for $V_C V_{Si}$, and we have confirmed that the energy differences are very small.
[79] D. J. Chadi and K. J. Chang, Phys. Rev. B **38**, 1523 (1988).
[80] A. Oshiyama, M. Saito, and O. Sugino, Appl. Surf. Sci. **85**, 239 (1995).
[81] S. K. Estreicher, J. L. Hastings, and P. A. Fedders, Appl. Phys. Lett. **70**, 432 (1997).
[82] J. L. Hastings, S. K. Estreicher, and P. A. Fedders, Phys. Rev. B **56**, 10215 (1997).
[83] A. Bongiorno, L. Colombo, and T. Diaz De la Rubia, Europhys. Lett. **43**, 695 (1998).
[84] T. Akiyama, A. Oshiyama, and O. Sugino, J. Phys. Soc. Jpn. **67**, 4110 (1998).
[85] A. Oshiyama and J.-i. Iwata, J. Phys. Conf. Ser. **302**, 012030 (2011).